

# A Statistical Model of Galaxies

Mattia Vaccari

Department of Astronomy, University of Padova  
Vicolo dell'Osservatorio 2, I-35122, Padova, Italy

CISAS "G. Colombo", University of Padova  
Via Venezia 15, I-35131, Padova, Italy  
vaccari@pd.astro.it

Erik Høg

Astronomical Observatory, University of Copenhagen  
Juliane Maries Vej 30, Dk-2100, Copenhagen Ø, Denmark  
erik@astro.ku.dk

GAIA-CUO-104      30 January 2002

## Abstract

Average optical properties of galaxies as available in recent literature are summarized. The differential and integral galaxy number density, the effective radius and the surface brightness profile of "typical" galaxies are given as function of the galaxy morphological type and total  $I$  magnitude, down to a limiting magnitude of  $I = 24$ .

These typical values are believed to be useful when only galaxy statistical properties, i.e. properties averaged over large galaxy samples, are of interest, e.g. when planning future large-scale surveys and data reduction undertakings.

A simple model giving the number and average photometric properties of galaxies as function of a limited set of parameters is useful for different purposes, e.g. in the planning of future galaxy observations, where it is required to estimate the number of galaxies that could be detected, the angular radius to which the surface brightness profile could be followed and the connected scientific yield.

The observations that are needed in order to build such a model are the number density, angular size and surface brightness distribution of the galaxies observed on the sky. Recent literature, and more specifically the Medium Deep Survey (MDS, Ratnatunga *et al.* (1999)) and Hubble Deep Field North (HDF-N, Williams *et al.* (1996)) databases obtained with the HST WFPC2 camera, offer a substantial amount of data in optical  $UBVRI$ -like bands, extending to large sky regions and faint magnitudes. The model's results, however, are here expressed in the  $I$  band, since mostly  $I$ -band data were used. A magnitude limit of  $I = 24$  mag was adopted as the best trade-off between the model's depth and reliability.

It turns out that, to a first approximation, the galaxy statistical properties that are here of interest can be conveniently expressed as function of two parameters only, namely the galaxy total magnitude and morphological type. It must be emphasized how, under our assumptions, these two parameters completely characterize the photometric properties of a galaxy. The predictions of our model are thus much different in nature from the results of conventional galaxy surface photometry analysis. While in the latter a set of parameters is fitted to galaxy images in order to obtain information about galactic structural properties, in our model the results of this analysis are combined to derive analytical expressions predicting the photometric properties of typical galaxies. While this model obviously cannot do justice to the strong individuality displayed by many galaxies, it is believed to yield sufficiently reliable results when only statistical properties, i.e. properties averaged over large samples, are of interest.

The results of this study have in fact been developed and used for the planning of future galaxy observations, namely to investigate the possibilities for multi-colour photometry of galaxies with the GAIA satellite (Perryman *et al.* (2001)). In this framework, they have proved a valuable tool e.g. in discussing the difficulties related to galaxy detection (Høg *et al.* (1999)) and observation (ESA (2000)). The model herein presented, as well as the tools developed for the simulation of galaxy observations and the performance expected from GAIA in this respect, are more thoroughly described in Vaccari (2000) and Vaccari (2001).

## 1 Morphological Classification

The classification of galaxies according to their shape is a fundamental tool in extragalactic astronomy. It is through classification schemes that astronomers identify how different types of galaxies are interrelated and thus build a deeper understanding of how galaxies form and evolve (van den Bergh (1998)). The most widely used galaxy classification scheme was first proposed by Hubble (1926) and later variously refined by Hubble himself and others. In its definitive form, described by Sandage (1961) and visually illustrated by the famous “tuning fork” diagram shown in Figure 1, Hubble’s scheme consists of four main morphological classes:

- Ellipticals (E) : elliptical galaxies are seen projected on the sky as more or less flattened ellipses, whose axis ratio roughly varies from 1 to 3. They have no particular substructure, and their surface brightness decreases very regularly from the center to the outer parts. They have no, or very little, interstellar matter, and a population of old stars. The effects of projection hinders us greatly in our attempts to determine the intrinsic shape of these galaxies, and the original long-standing hypothesis of an axysymmetric ellipsoidal structure has recently been questioned.
- Lenticulars (S0) : lenticular galaxies consist of at least two components, namely a central stellar concentration, or bulge, structurally similar to an elliptical galaxy, and a rather flat stellar disk that shows no sign of spiral structures. In addition, they sometimes contain a bar-shaped stellar component crossing the galactic nu-

cleus. Like E galaxies, they have little interstellar matter and a population of old stars.

- Spirals (S) : spiral galaxies consist of a stellar bulge, sharing the characteristics of an elliptical galaxy, and of a disk containing young stars, significant amounts of interstellar matter and a more or less well-defined spiral pattern. They can also contain a bar-like component as well as more unusual structures like rings and lenses, whose composition is similar, in general, to that of the disk component.
- Irregulars (Irr) : irregular galaxies are galaxies that cannot be classified in the three previous classes, usually owing to their lack of symmetry or of well-defined spiral arms. They frequently display structures like dust lanes or bright knots containing O and B stars.

These four basic classes can be divided into several further subclasses, but these finer distinctions will not be considered here.

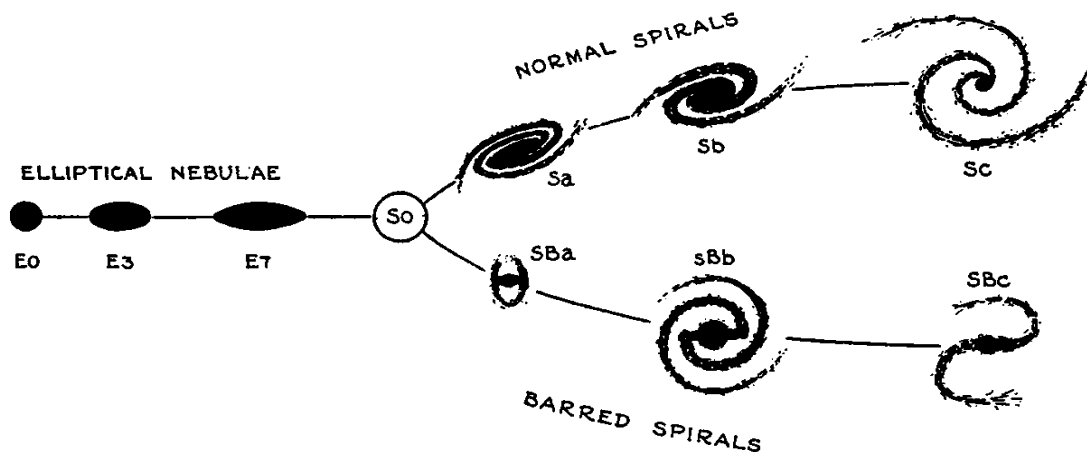


Figure 1: An early version of Hubble’s galaxy classification scheme of regular galaxies, also known as the “tuning fork” diagram. Reproduced from Hubble (1936).

As for the relative frequencies of the different morphological types, in recent years they have been extensively investigated via both visual and automated classification procedures. In particular, deep observation campaigns carried out with the HST, namely the Medium Deep Survey (MDS) and the Hubble Deep Field North (HDF-N), have proved that when such frequencies are calculated over magnitude-limited samples of different depths, then they strongly depend on the limiting magnitude, showing a sharp decrease in the number of spirals and an increase in the number of ellipticals and unclassifiable galaxies at faint magnitudes. Relative frequencies of morphological types in magnitude-limited samples of different limiting magnitudes are given in Table 1.

In Section 4 regular galaxies are divided into two classes, namely elliptical galaxies (E) and disk galaxies (D), on the basis of their surface brightness distribution. Taken

Table 1: Relative frequencies of DDO morphological types in magnitude-limited samples of different limiting magnitude. SAC stands for Shapley-Ames Catalog (Shapley and Ames (1932)), MDS for Medium Deep Survey (Ratnatunga *et al.* (1999)) and HDF-N for Hubble Deep Field North (Williams *et al.* (1996)), from Table 2 in van den Bergh *et al.* (1996). Morphological classifications from van den Bergh (1960), Abraham *et al.* (1996b) and Abraham *et al.* (1996a), respectively. Wider DDO classification bins (E, S0, S, Ir and Unclassified) are indicated by horizontal lines. Note that the SAC makes no distinction between E, E/S0 and S0, and that for the MDS and HDF data, only galaxies with  $I$  less than 21 and 24, respectively, were considered, in order to obtain a truly magnitude-limited sample and thus more robust estimates.

Type	SAC	MDS	HDF-N
E		16.6	23.9
E/S0	22.2	3.3	0.7
S0		6.9	4.3
S0/Sa	0.0	0.0	0.7
E/Sa	1.3	0.0	1.4
Sa	6.9	7.5	14.6
Sab	0.2	3.1	1.4
Sb	26.9	7.1	4.3
Sbc	0.3	4.0	0.0
Sc	22.9	12.8	1.4
S	10.0	14.6	13.2
Sc/Ir	0.2	0.9	0.0
Ir	2.0	6.4	2.5
Unclassified	7.0	16.8	31.4

the MDS frequencies from Table 1 as representative, it can be concluded that the relative frequencies of these two classes are of about 20% and 80% for E and D galaxies, respectively.

## 2 Number Counts

Galaxy differential number counts, giving the number of galaxies per unit sky area per unit magnitude interval as function of total magnitude, have always been a classical tool of observational cosmology. Consequently, a great effort has always been devoted to the extension of the observations to deeper magnitudes, larger sky regions and a wider range of colors. In particular, in the past few years  $I$ -band counts at high Galactic latitudes have been reliably extended down to  $I \simeq 24$ , as summarized e.g. by Shimasaku and Fukugita (1998). In our model, counts from three different sources were combined in order to cover as large a magnitude range as possible. At bright magnitudes, i.e. for  $I \leq 19$ , well-established counts were provided by Lattanzi (1997), whereas at fainter magnitudes results from Glazebrook *et al.* (1995) ( $19 < I < 21$ ) and

Abraham *et al.* (1996a) ( $21 < I < 24$ ) were used. A least-square polynomial fit in  $\log N$  vs.  $I$  was performed on these data, in order to assess the consistency of the three sources and to obtain a functional form  $N = N(I)$  for use in the following. It was thus found that a second degree polynomial was sufficient to obtain a good fit to the data. The number counts and the best-fit parabola are shown in Figure 2, while the best-fit parameters are given in Table 2. According to this approximation, the differential number counts take the following functional form

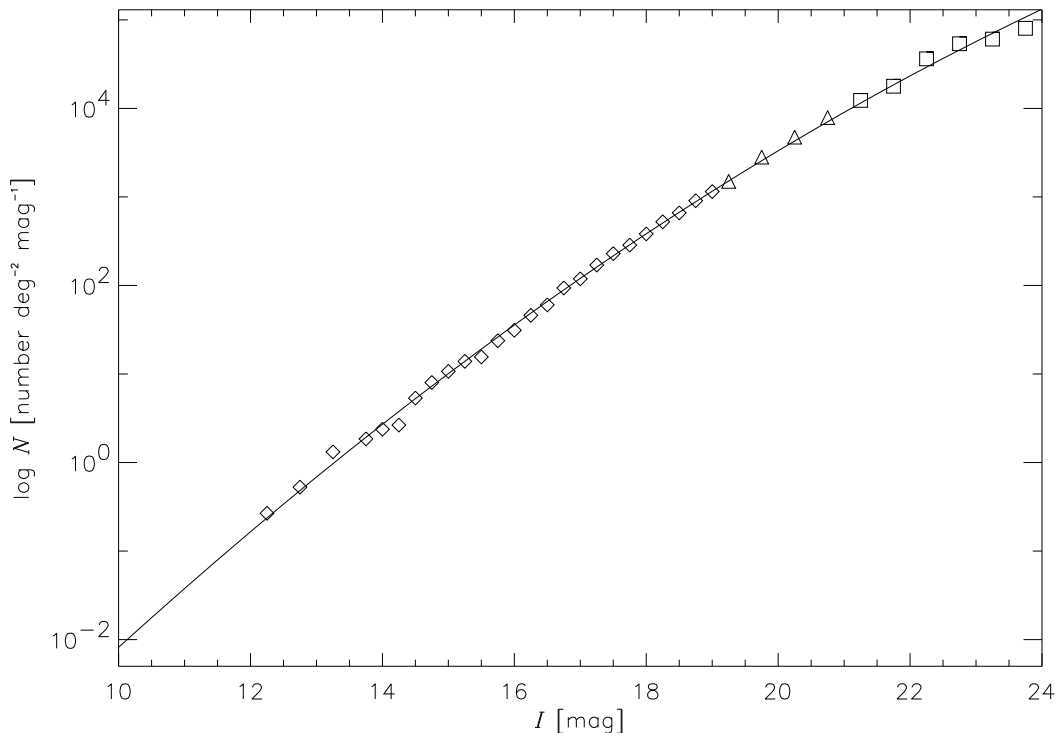


Figure 2: Galaxy differential number counts in the  $I$ -band. Data points from Lattanzi (1997) (diamonds), Glazebrook *et al.* (1995) (triangles) and Abraham *et al.* (1996a) (squares). The solid line shows the least-square second degree polynomial best-fit.

$$N(I) = \text{dex}(a_N + b_N I + c_N I^2) \quad [\text{number deg}^{-2} \text{ mag}^{-1}], \quad (1)$$

where “dex” stands for the exponential function in base ten.

Values of the three parameters contained in Equation 1 are given in Table 2, while counts calculated with this formula are given in Table 4.

The cumulative galaxy number counts, giving the total number of galaxies per unit sky area brighter than a given  $I$  magnitude  $I_c$ , are then given by the definite integral

$$N_c(I) = \int_{-\infty}^I N dI' \quad [\text{number deg}^{-2}]. \quad (2)$$

Table 2: Parameters of  $\log N$  vs.  $I$  least-square second-degree polynomial best-fit.  $N$  expressed in number  $\text{deg}^{-2} \text{mag}^{-1}$ .

$a_N$	$b_N$	$c_N$
-9.9942	0.90564	-0.011493

Since the function given by Equation 1 does not have an analytic antiderivative, Romberg numerical integration (see Chapter 4 in Press *et al.* (1992)), was performed. Cumulative galaxy number counts that were thus obtained are listed in Table 4.

### 3 Angular Size

Since galaxies are not sharp-edged objects, their angular size can be variously defined (see Mihalas and Binney (1981) and Binney and Merrifield (1998)). As far as studies of surface brightness distribution are concerned, however, the parameter most widely used to characterize the size of a galaxy is its effective radius. This can be roughly defined as the radius encircling half of the light emitted by the galaxy, but in practice its measurement is usually performed through a more complicated process.

Surface photometry of galaxies (see e.g. Jedrzejewski (1987) for E galaxies and Kent (1985) for D galaxies) is usually analysed by fitting ellipses to the isophotes and by plotting their surface brightness versus their radius, which is defined as the geometric mean of the ellipse's semi-axes  $a$  and  $b$ , i.e.  $r = \sqrt{ab}$ . The resulting plot is then called the surface brightness radial profile of the galaxy. In this context, the effective radius of the galaxy is defined as the radius of the isophote encircling half of the light emitted by the galaxy, also called the effective isophote. The effective radius and the effective surface brightness, the latter being the surface brightness of the effective isophote, are usually indicated with  $r_e$  and  $\mu_e$ , respectively.

Until the launch of HST, accurate measurements of the small angular sizes of faint galaxies were made virtually impossible by the phenomenon of seeing. The Medium Deep Survey (Ratnatunga *et al.* (1999)), the first survey project to be carried out with HST superb instrumentation, has recently brought to an end this long-standing lack of meaningful data, while Im *et al.* (1995) have demonstrated the potential of angular size measurements to discriminate between currently competing cosmological models.

Casertano *et al.* (1995) have obtained effective radii for about 10,000 galaxies from Wide Field and Planetary Camera (WF/PC) parallel observations of random fields in the  $I$  band. As shown in their Figure 6, the observed angular size distribution as function of  $I$  magnitude shows a large scatter about the median value, mainly due to the intrinsic scatter in linear size and redshift distribution. The same figure also shows that the observed relation between the median effective radius and  $I$  magnitude is well-fit by the theoretically predicted relation for galaxies of constant central surface brightness  $\mu_0 = 19.3 \text{ mag/arcsec}^2$  and absolute magnitude  $M_I = -20.5$  in the context of a mild luminosity evolution scenario. This latter relation asymptotically approaches the linear relation in  $\log r_e$  vs.  $I$  that is measured in local samples of bright spiral galaxies following

Freeman’s law, and was therefore taken as a description of the relation between the galaxy effective radius and magnitude in our model. Least-square polynomial fit showed that its accurate description required a fourth-degree polynomial, which is represented in Figure 3, together with the Euclidean extrapolation to faint magnitudes of the local linear relation. The relation that in the following will be used to express  $r_e$  as function

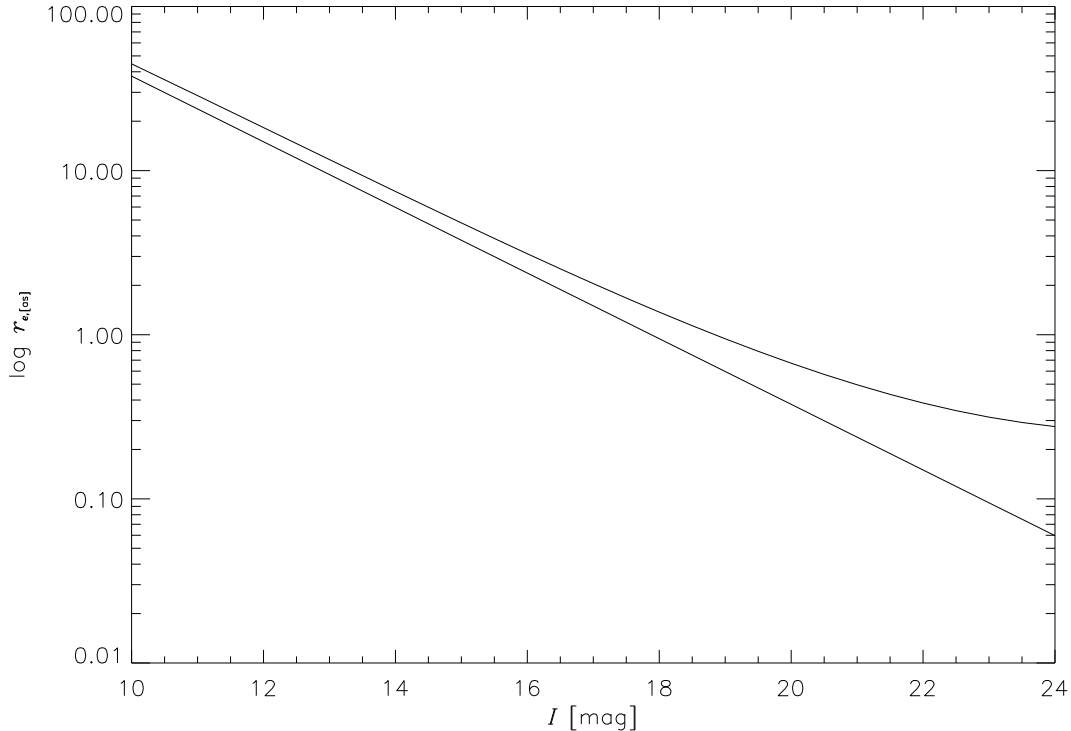


Figure 3: Median galaxy effective radius in the  $I$  band. The straight line represents the Euclidean extrapolation to faint magnitudes of the result valid for local samples of spiral galaxies following Freeman’s law, while the curve represents the best fourth-degree polynomial fit to the theoretically predicted relation that best fits the observations at faint magnitudes. Note the pronounced divergence of the two curves for  $I \gtrsim 19$ . From Casertano *et al.* (1995).

of  $I$  is therefore

$$r_e(I) = \text{dex}(a_r + b_r I + c_r I^2 + d_r I^3 + e_r I^4) \quad [\text{arcsec}] . \quad (3)$$

The values of the five parameters contained in Equation 3 are given in Table 3. Note that it is assumed not only that  $r_e$  depends on  $I$  only, but also that the same relation holds for all galaxies, irrespective of their morphological types. From a statistical point of view, however, and as far as Equation 3 holds on average, the net effect on the total number of detected galaxies should be negligible. Effective radii calculated from

Table 3: Parameters of  $\log r_e$  vs.  $I$  least-square fourth-degree polynomial best-fit.  $r_e$  expressed in arcsec.

$a_r$	$b_r$	$c_r$	$d_r$	$e_r$
$3.57702 \cdot 10^0$	$-2.12805 \cdot 10^{-1}$	$5.34616 \cdot 10^{-3}$	$-4.62001 \cdot 10^{-4}$	$1.28947 \cdot 10^{-5}$

Equation 3, are given in Table 4. A rough estimation of the typical surface brightness of the central regions of galaxies can be given by the average surface brightness inside the effective radius  $\langle \mu \rangle_e$ . Under our assumptions, and from the definition of effective radius, this quantity is equal for Es and Ds and can be written as

$$\begin{aligned} \langle \mu \rangle_e &= -2.5 \log \left( \frac{F/2}{\pi r_e^2 \Sigma_{zp}} \right) = -2.5 \log \left( \frac{F_{zp} \text{dex}(-0.4 I)}{\Sigma_{zp} 2\pi r_e^2(I)} \right) = \\ &= 2.5 \log(2\pi) + 5 \log(r_{e,[\text{as}]}(I)) + I_{[\text{mag}]} \quad [\text{mag/arcsec}^2]. \end{aligned} \quad (4)$$

Values of  $\langle \mu \rangle_e$  are given in Table 5. To characterize the total fraction of the sky occupied by galaxies brighter than a given magnitude, one can define  $\Omega_e$  as the total solid angle that lies within the effective radius of all galaxies brighter than a given magnitude. Since superposition of different galaxies on the same sky regions is negligible, at least in the magnitude range we are considering,  $\Omega_e$  can simply be written as

$$\begin{aligned} \Omega_e(I) &= \frac{\Omega_{sky}}{60^4} \int_{-\infty}^I \pi r_e^2(I') N(I') dI' = [\text{Equations 1 and 3}] = \\ &= \frac{\pi \Omega_{sky}}{60^4} \int_{-\infty}^I \text{dex} [(2a_r + a_N) + (2b_r + b_N) I' + (2c_r + c_N) I'^2 + 2d_r I'^3 + 2e_r I'^4] dI', \end{aligned} \quad (5)$$

where  $\Omega_{sky}$  is the solid angle spanned by the whole sky and the factor  $60^4$  was introduced to take into account the fact that the coefficients giving  $N$  and  $r_e$  as function of  $I$  in Equations 1 and 3 are expressed in different angular units. Values of  $\Omega_e/\Omega_{sky}$ , calculated through Romberg integration of Equation 5, are given in Table 4.

## 4 Surface Brightness Distribution

As explained in Section 3, the two-dimensional surface brightness distribution of a galaxy is usually analysed so as to produce a one-dimensional radial profile. It turns out that the different physical components of galaxies have characteristic radial profiles, so that it is possible to model the radial profiles of different classes of galaxies as sums of different components.

Following Binney and Merrifield (1998), as far as surface brightness radial profiles are concerned, we shall here distinguish only two classes of typical galaxies, namely the elliptical galaxies (E) and disk Galaxies (D), where the latter class include spirals and lenticulars. While elliptical galaxies will be modelled as made of a bulge component only, disk galaxies will be considered as the combination of a bulge and a disk component. In both cases, galaxy images are assumed circularly symmetric. Note that all data



Table 4: Number and size of galaxies according to our statistical model. Modelled differential and cumulative number counts, effective radius and fraction of sky inside the effective radius at different  $I$ .

$I$ mag	$N$ deg <sup>-2</sup> mag <sup>-1</sup>	$N_c$ deg <sup>-2</sup>	$r_e$ arcsec	$\Omega_e/\Omega_{sky}$ 10 <sup>-6</sup> sky
10	0.008183	0.005151	44.72	5.350
11	0.03777	0.02458	28.64	10.93
12	0.1654	0.1114	18.29	21.15
13	0.6867	0.4791	11.68	38.88
14	2.705	1.958	7.468	68.08
15	10.10	7.596	4.801	114.0
16	35.79	27.99	3.115	183.6
17	120.3	98.00	2.049	285.9
18	383.3	325.9	1.374	433.3
19	1159	1030	0.9446	644.0
20	3322	3093	0.6707	946.5
21	9032	8826	0.4954	1389
22	23290	23940	0.3838	2060
23	56970	61760	0.3147	3132
24	132200	151500	0.2758	4969

and modelled numerical values are given in the  $I$  band, but that the subscript  $I$  will be here dropped for convenience from most formulae. Note also that the derivation of the mathematical results and the description of the notation used in the following are given in the Appendix.

#### 4.1 Elliptical Galaxies

The surface brightness radial profiles of elliptical galaxies are in general reasonably well described by de Vaucouleurs, or  $r^{1/4}$ , law, first introduced by de Vaucouleurs (1948)

$$\Sigma_E(r) = \Sigma_{E,e} \exp \left( -7.6692 \left[ \left( \frac{r}{r_e} \right)^{1/4} - 1 \right] \right), \quad (6)$$

where the effective surface brightness is labelled with an additional “ $E$ ” because in our model this quantity, unlike the effective radius, will in general be different for E and D galaxies. This law has succeeded in reproducing, with a remarkable accuracy, the profiles of quite a few E galaxies. For instance, Capaccioli *et al.* (1990) found that the  $r^{1/4}$  fit of the surface brightness radial profile of the nearby standard elliptical NGC 3379 give residuals smaller than 0.08 mag over a 10 magnitude range. Makino *et al.* (1990), however, found from dynamical arguments that the  $r^{1/4}$  law bore little physical significance, though it is the best-fitting function, and that  $r^{1/n}$  laws with  $n$  in the range 3–10 gave almost as good fits for a range of  $r$  of about 100. More recently, Caon *et al.*

(1993) showed that the best-fitting  $n$  correlates with the galaxy linear effective radius and luminosity, while Andredakis *et al.* (1995) found that the light profiles of the bulges of disk galaxies, which are also usually modelled with an  $r^{1/4}$  law, are in fact best-fitted by  $r^{1/n}$  profiles with an  $n$  correlating with the galaxy morphological type. Nevertheless, the empirical fitting function given by Equation 6 is useful for characterizing the global properties of galaxies, and by that token in this study elliptical galaxies and bulges of disk galaxies will both be modelled with  $r^{1/4}$  laws.

On a magnitude scale, Equation 6 becomes

$$\mu_E(r) = \mu_{E,e} + 8.3268 \left[ \left( \frac{r}{r_e} \right)^{1/4} - 1 \right], \quad (7)$$

where  $\mu_{E,e}$  is the effective surface brightness of Es expressed in mag/arcsec<sup>2</sup>. This latter quantity can be expressed as function of  $r_e$  and  $I$ , and thus, via Equation 3, of  $I$  only, obtaining

$$\mu_{E,e} = 2.5 \log(22.665) + 5 \log(r_{e,[as]}(I)) + I_{[mag]} \quad [\text{number deg}^{-2} \text{ mag}^{-1}]. \quad (8)$$

Values of  $\mu_{E,e}$  are given in Table 5.

## 4.2 Disk Galaxies

As first suggested by de Vaucouleurs (1959), the surface brightness radial profile of disk galaxies can be interpreted as the sum of two components, the so called bulge component following the  $r^{1/4}$  law and the so called disk component following the exponential law

$$\Sigma_d(r) = \Sigma_0 \exp\left(-\frac{r}{r_s}\right), \quad (9)$$

where  $\Sigma_0$  is the central surface brightness and  $r_s$  is the so called disk scale length. Equation 9 can be rewritten in a form similar to the one used for the  $r^{1/4}$  law as

$$\Sigma_d(r) = \Sigma_e \exp\left[-1.6783 \left(\frac{r}{r_e} - 1\right)\right], \quad (10)$$

where

$$\Sigma_0 = 5.3567 \Sigma_e, \quad r_s = \frac{r_e}{1.6783}. \quad (11)$$

Since the first systematic study of Freeman (1970), this law has been known to fit the profiles of the outer regions of a large class of disk galaxies and has, in fact, come to define the typical surface brightness profile of the intrinsically flat component of disk galaxies, to the extent that deviations from these profile are generally ascribed to the existence of other components or to the effects of dust. Assuming this analytical form for the profile of the disk component, one can then try to disentangle the contributions of the bulge and disk components by means of fitting techniques. The methods for doing this have in time undergone a great development, from the simple one-dimensional

fitting procedure along the galaxy major axis first adopted by Freeman (1970) to the bidimensional decomposition techniques currently being developed, which are applied to whole galaxy images (see e.g. Byun and Freeman (1995)). In this study, a bulge+disk profile will be considered, combining an  $r^{1/4}$  law with an exponential law, thus not considering contributions from components such as spiral arms, bars, rings, lenses, or the photometric effects of dust. The most general form of such a profile

$$\begin{aligned}\Sigma_D(r) &= \Sigma_b(r) + \Sigma_d(r) = \\ &= \Sigma_{b,e} \exp\left(-7.6692 \left[\left(\frac{r}{r_{b,e}}\right)^{1/4} - 1\right]\right) + 5.3567 \Sigma_{d,e} \exp\left(-\frac{1.6783 r}{r_{d,e}}\right),\end{aligned}\quad (12)$$

depends on two pairs of parameters characterizing the bulge and disk components, respectively. The only independent variable we have so far introduced in our model is the total magnitude, which however determines also the effective radius through Equation 3. Therefore, the values of two other parameters must be given in order to completely determine the form of Equation 12. A convenient choice are two quantities derived from bulge/disk decompositions and frequently reported in the literature, namely the bulge/bulge+disk ratio  $B/T$ , or the ratio between the brightness contributed by the bulge component and the total brightness, and the ratio  $r_{b,e}/r_{d,e}$  between the effective radii of the bulge and disk components. As shown in the Appendix, these two parameters completely determine the bulge+disk profile. As for  $B/T$ , Kent (1985) found that in intrinsically luminous D galaxies this is tightly correlated with the morphological type, falling from a mean value of 0.65 for S0 to a mean value of 0.15 for Sc and later types. Recently, Ratnatunga *et al.* (1999) found a mean  $B/T$  of 0.4 from the bulge/disk decomposition of the MDS galaxies. The same two references then agree in fixing to about 0.5 the mean value of  $r_{b,e}/r_{d,e}$ . Such an excellent agreement between parameters obtained from galaxies of largely different magnitudes suggested to consider the two parameters as fixed, without introducing in the model the complications of other free parameters. Values of  $B/T = 0.4$ , corresponding to a bulge/disk ratio  $B/D = 0.666$ , and  $r_{b,e}/r_{d,e} = 0.5$  were therefore assumed. With our choices for  $B/T$  and  $r_{b,e}/r_{d,e}$  the bulge+disk profile becomes

$$\begin{aligned}\Sigma_D(r) &= \Sigma_b(r) + \Sigma_d(r) = \\ &= 0.76931 \Sigma_{D,e} \exp\left(-7.6692 \left[\left(\frac{1.6617 r}{r_e}\right)^{1/4} - 1\right]\right) + 2.9343 \Sigma_{D,e} \exp\left(-\frac{1.3945 r}{r_e}\right).\end{aligned}\quad (13)$$

In general, the bulge and disk components dominate the profile at small and large radii, respectively. Note, however, that due to the analytical form of the two profiles, at very large radii the bulge contribution eventually exceeds that of the disk. In fact, practically all (99%) of the brightness predicted by the disk profile falls within 4 effective radii, but for the bulge profile only 85% of the light is within 4 effective radii, and the model needs to extend out to about 19 effective radii to contain 99% of it. Shifting to a magnitude scale, the analytical expression for  $\mu_D$  is not as simple as that derived for ellipticals and is

$$\mu_D(r) = \mu_{D,e} - 2.5 \log \left[ 0.76931 \exp\left(-7.6692 \left[\left(\frac{1.6617 r}{r_e}\right)^{1/4} - 1\right]\right) + 2.9343 \exp\left(-\frac{1.3945 r}{r_e}\right) \right].\quad (14)$$

The total brightness emitted by the galaxy and the effective surface brightness can be written as

$$F_{D,tot} = 15.796 \Sigma_{D,e} r_e^2, \quad (15)$$

and

$$\mu_{D,e} = 2.5 \log(15.796) + 5 \log(r_{e,[as]}) + I_{[mag]} \quad [\text{number deg}^{-2} \text{ mag}^{-1}]. \quad (16)$$

Table 5 reports the values of  $\langle \mu \rangle_e$ ,  $\mu_{E,e}$  and  $\mu_{D,e}$  for different total  $I$  magnitudes.

Table 5: Representative surface brightness levels of galaxies according to Equations 4, 8 and 16. Average inside the effective radius and at that radius for E and D galaxies. As discussed in Section 2, D galaxies are four times more frequent than E galaxies.

$I$ mag	$\langle \mu \rangle_e$ mag/arcsec <sup>2</sup>	$\mu_{E,e}$ mag/arcsec <sup>2</sup>	$\mu_{D,e}$ mag/arcsec <sup>2</sup>
10	20.2481	21.6410	21.2490
11	20.2800	21.6730	21.2809
12	20.3067	21.6996	21.3076
13	20.3321	21.7250	21.3330
14	20.3616	21.7545	21.3625
15	20.4023	21.7952	21.4032
16	20.4628	21.8557	21.4637
17	20.5531	21.9461	21.5540
18	20.6851	22.0780	21.6860
19	20.8718	22.2648	21.8727
20	21.1281	22.5210	22.1290
21	21.4702	22.8632	22.4711
22	21.9161	23.3090	22.9170
23	22.4851	23.8780	23.4860
24	23.1981	24.5911	24.1991

## 5 Model's Validity and Verifications

As it was variously stressed, a model such as that here described cannot accurately describe the properties of any given galaxy. However, it is expected to hold on average, i.e. when the average properties of a representative sample of galaxies are considered. Given the several rough approximations introduced, the question as to which extent the model is quantitatively reliable for the purpose of the planning of future galaxy observations cannot be answered without a direct comparison between predicted and observed profiles. Before carrying out such a comparison, we will however make a few, essentially qualitative considerations about the model's general validity.

Roughly speaking, it is expected that our statistical model will reliably describe the surface brightness radial profiles of faint galaxies, while the brightest galaxies will

display a stronger individuality and thus will require more realistic surface brightness distribution functions to be considered. This latter class of galaxies may tentatively be estimated to include all the galaxies in the Shapley-Ames Catalog (Shapley and Ames (1932)), so about a thousand galaxies. These galaxies can display a very complex structure and be of very large angular extent, e.g. about 10 deg for the Large Magellanic Cloud, and thus require individual consideration. At fainter magnitudes, only the overall structure of galaxies will be relevant, and the typical properties predicted by our model will be useful.

As for a quantitative evaluation of model's reliability, a comparison between its predictions and some ground-based surface photometry of bright galaxies taken from the literature was carried out. Even though, owing to seeing, ground-based observations do not allow an accurate determination of the profiles in the galaxy innermost regions, they have the advantages of being available in substantial amounts and of frequently following the brightness profiles to very large radii. Conversely, space observations cover a small field of view, have mostly low exposure times and are still limited in quantity. In much the same way, the large availability in the literature of  $B$ -band profiles extending down to large radii suggested the use of these for model's verification. The conversions between  $B$  and  $I$  was carried out using the constant color index  $B - I = 2.0$ , and correspondingly  $\mu_B - \mu_I = 2.0$ , which is the average value for bright galaxies according to Prugniel and Héraudeau (1998). Thus, in order to obtain the predicted  $B$ -band brightness profile against which observations could be compared, the measured total  $B$  magnitude of the galaxy is transformed to  $I$  through the  $I = B - 2.0$ . Then the predicted  $I$ -band profile can be derived as described in Sections 4.1 and 4.2, for Es and Ds respectively. Finally, the predicted  $B$ -band brightness profile is derived through the  $\mu_B = \mu_I + 2.0$ .

For elliptical galaxies, the model's predictions were compared with the composite CCD-photographic brightness profiles obtained by Capaccioli *et al.* (1988). for 9 galaxies in the ranges  $10.5 < B < 12.7$  and  $18 < \mu_B < 28$  and down to radii of about 250 arcsec. These are typically found to agree with our model within 0.2 mag/arcsec<sup>2</sup> outside an inner circular area of radius about 1 arcsec. Within this area, the observed profiles show a sharp flattening which our model does not describe properly so that the predicted profile is systematically brighter than the observations. This is clearly due to the phenomenon of seeing and is compensated by the observed profiles being systematically brighter than predicted at radii just above 1 arcsec.

For disk galaxies, the model's predictions were compared with the photographic surface photometry obtained by Boroson (1981) for 26 galaxies in the ranges  $8.5 < B < 12.5$  and  $18 < \mu_B < 26$  and down to radii of 120–240 arcsec. In this case, the observations are typically found to agree with the predicted profiles within 0.3 mag/arcsec<sup>2</sup> outside the 1-arcsec radius circular area where seeing flattens the observed profiles as observed in the ellipticals.

## 6 Conclusions

On the whole, it can be concluded that our model predicts the galaxy surface brightness radial profiles over a large range of radii with an accuracy of about 30% for most galaxies. Such an accuracy in the model's predictions must be considered satisfactory in most cases in view of its application to the planning of future galaxy observations.

## A Galaxy Surface Brightness Radial Profiles

### A.1 Sersic Law

The properties of galaxy surface brightness radial profiles can be derived in a general form using Sersic law, first introduced by Sersic (1968) and also known as  $r^{1/n}$  law or generalized de Vaucouleurs law. This can be written as

$$\Sigma(r) = \Sigma_e \exp \left( -b_n \left[ \left( \frac{r}{r_e} \right)^{1/n} - 1 \right] \right), \quad (17)$$

where  $r_e$  is the effective radius, or the radius within which the galaxy emits half its brightness,  $\Sigma_e$  is the surface brightness at  $r_e$  and  $b_n$  is a positive parameter that, for a given  $n$ , can be determined from the definition of  $r_e$  and  $\Sigma_e$ . The value of  $n$  determines the degree of concentration of the profile, quantified e.g. by the fraction of energy emitted within a given number of effective radii, the profile being steeper or less concentrated for higher  $n$  and conversely flatter or less concentrated for lower  $n$ . Particularly interesting special cases are the bulge-like  $r^{1/4}$  profile for  $n = 4$  and the disk-like exponential profile for  $n = 1$ , which will be discussed in greater detail in Sections A.2 and A.3.

According to Equation 17, the brightness integrated within a given radius  $r$  is given by

$$\begin{aligned} F(r) &= \int_0^r 2\pi r' \Sigma(r') dr' = 2\pi \Sigma_e \int_0^r r' \exp \left( -b_n \left[ \left( \frac{r'}{r_e} \right)^{1/n} - 1 \right] \right) dr' = \\ &= 2\pi \exp(b_n) \Sigma_e \int_0^r r' \exp \left[ -b_n \left( \frac{r'}{r_e} \right)^{1/n} \right] dr' = \left[ r'' \equiv b_n \left( \frac{r'}{r_e} \right)^{1/n} \right] = \\ &= 2\pi \exp(b_n) \Sigma_e \int_0^{b_n \left( \frac{r}{r_e} \right)^{1/n}} \frac{r_e}{b_n^n} r'' \exp(-r'') \frac{n r_e}{b_n^n} r''^{(n-1)} dr'' = \\ &= 2\pi \frac{n \exp(b_n)}{b_n^{2n}} \Sigma_e r_e^2 \int_0^{b_n \left( \frac{r}{r_e} \right)^{1/n}} r''^{(2n-1)} \exp(-r'') dr'' = \\ &= 2\pi \frac{n \exp(b_n)}{b_n^{2n}} \Sigma_e r_e^2 \gamma \left( 2n, b_n \left( \frac{r}{r_e} \right)^{1/n} \right), \end{aligned} \quad (18)$$

where  $\gamma$  is the incomplete gamma function. The total brightness predicted by the profile

is

$$\begin{aligned}
F_{tot} &= \lim_{r \rightarrow \infty} F(r) = 2\pi \frac{n \exp(b_n)}{b_n^{2n}} \Sigma_e r_e^2 \lim_{x \rightarrow \infty} \gamma(2n, x) = \\
&= 2\pi \frac{n \exp(b_n)}{b_n^{2n}} \Sigma_e r_e^2 \Gamma(2n) \equiv k_n \Sigma_e r_e^2 ,
\end{aligned} \tag{19}$$

where  $\Gamma$  is the gamma function. This relation, remembering that, by definition of effective radius, it is  $F(r_e) = F_{tot}/2$ , can be used to obtain an equation linking  $b_n$  and  $n$ . After cancellation of common terms, one obtains

$$\Gamma(2n) - 2\gamma(2n, b_n) = 0 , \tag{20}$$

a non-linear equation which can only be solved numerically, e.g. via the Newton method (see Section 9.7 in Press *et al.* (1992)). Values of  $b_n$  and  $k_n$  corresponding to integer values of  $n$  from 1 to 10 are given in Table 6.

Table 6: Values of  $b_n$  and  $k_n$  for different values of  $n$ .

$n$	$b_n$	$k_n$
1	1.6783470	11.948495
2	3.6720608	16.310881
3	5.6701554	19.743758
4	7.6692495	22.665234
5	9.6687149	25.251949
6	11.668363	27.597728
7	13.667757	29.759676
8	15.667704	31.774676
9	17.667636	33.669429
10	19.667567	35.463170

## A.2 Bulge Profile

For  $n = 4$ , Equation 17 becomes de Vaucouleurs, or  $r^{1/4}$ , law

$$\Sigma_b(r) = \Sigma_e \exp \left( -7.6692 \left[ \left( \frac{r}{r_e} \right)^{1/4} - 1 \right] \right) , \tag{21}$$

which characterizes the profiles of elliptical galaxies and bulge components of disk galaxies. According to this profile, the total brightness can be written as

$$F_{b,tot} = 22.665 \Sigma_e r_e^2 , \tag{22}$$

while the central surface brightness  $\Sigma_0$  and the average surface brightness inside the effective radius  $\langle \Sigma \rangle_e$  are related to  $\Sigma_e$  by

$$\Sigma_0 = 2141.4 \Sigma_e , \quad \langle \Sigma \rangle_e = \frac{F_{b,tot}/2}{\pi r_e^2} = 3.6072 \Sigma_e . \tag{23}$$

The bulge profile given by Equation 21 can be put on the more common logarithmic scale writing

$$\begin{aligned}\mu_b(r) &= -2.5 \log \left( \frac{\Sigma_b(r)}{\Sigma_{zp}} \right) = -2.5 \log \left( \frac{\Sigma_e}{\Sigma_{zp}} \right) - \frac{2.5}{\ln 10} \left( -7.6692 \left[ \left( \frac{r}{r_e} \right)^{1/4} - 1 \right] \right) = \\ &= \mu_e + 8.3268 \left[ \left( \frac{r}{r_e} \right)^{1/4} - 1 \right] \text{ [mag arcsec}^{-2}\text{]} ,\end{aligned}\tag{24}$$

where  $\Sigma_{zp}$  is the zero-point of the adopted surface brightness magnitude scale. Similarly, Equation 22 can be manipulated so as to express  $\Sigma_e$  as function of  $r_e$  and  $I$ , obtaining

$$\begin{aligned}\mu_e &= -2.5 \log \left( \frac{\Sigma_e}{\Sigma_{zp}} \right) = -2.5 \log \left( \frac{F_{zp} \text{dex}(0.4 I)}{k_4 \Sigma_{zp} r_e^2} \right) = \\ &= 2.5 \log(k_4) + 5 \log(r_{e,[\text{as}]}) + I_{[\text{mag}]} \text{ [mag arcsec}^{-2}\text{]} ,\end{aligned}\tag{25}$$

where  $F_{zp}$  is the zero-point of the adopted brightness magnitude scale.

### A.3 Disk Profile

For  $n = 1$ , Equation 17 can be rewritten as the exponential law

$$\begin{aligned}\Sigma_d(r) &= \Sigma_e \exp \left[ -1.6783 \left( \frac{r}{r_e} - 1 \right) \right] = \exp(1.6783) \Sigma_e \exp \left( -\frac{1.6783}{r_e} r \right) \\ &= 5.3567 \Sigma_e \exp \left( -\frac{r}{r_e/1.6783} \right) = \Sigma_0 \exp \left( -\frac{r}{r_s} \right) ,\end{aligned}\tag{26}$$

which characterizes the profile of disk components of disk galaxies, where  $\Sigma_0$  is the central surface brightness and  $r_s$  is referred to as the disk scale length. The relations between these two quantities and  $\Sigma_e$  and  $r_e$  are respectively

$$\Sigma_0 = 5.3567 \Sigma_e , \quad r_s = \frac{r_e}{1.6783} .\tag{27}$$

According to this profile, the total brightness of the galaxy can be written as

$$F_{d,tot} = 11.948 \Sigma_e r_e^2 ,\tag{28}$$

while the average surface brightness inside the effective radius  $\langle \Sigma \rangle_e$  is related to  $\Sigma_e$  by

$$\langle \Sigma \rangle_e = \frac{F_{d,tot}/2}{\pi r_e^2} = 1.9016 \Sigma_e .\tag{29}$$

When put on a magnitude scale, the disk profile given by Equation 26 becomes

$$\begin{aligned}\mu_d(r) &= -2.5 \log \left( \frac{\Sigma_d(r)}{\Sigma_{zp}} \right) = -2.5 \log \left( \frac{\Sigma_e}{\Sigma_{zp}} \right) - \frac{2.5}{\ln 10} \left[ 1.6783 \left( \frac{r}{r_e} - 1 \right) \right] = \\ &= \mu_e + 1.8224 \left( \frac{r}{r_e} - 1 \right) \text{ [mag arcsec}^{-2}\text{]} ,\end{aligned}\tag{30}$$



while Equation 28 can be trivially manipulated to obtain for  $\Sigma_e$  the expression

$$\begin{aligned}\mu_e &= -2.5 \log \left( \frac{\Sigma_e}{\Sigma_{zp}} \right) = -2.5 \log \left( \frac{F_{zp} \text{dex}(0.4 I)}{k_1 \Sigma_{zp} r_e^2} \right) = \\ &= 2.5 \log(k_1) + 5 \log(r_{e,[\text{as}]}) + I_{[\text{mag}]} \quad [\text{mag arcsec}^{-2}] .\end{aligned}\quad (31)$$

#### A.4 Bulge+Disk Profile

The surface brightness radial profiles of disk galaxies are usually modelled as the sum of a bulge and a disk component. The resulting bulge+disk profile can in general be written as

$$\begin{aligned}\Sigma_{b+d}(r) &= \Sigma_b(r) + \Sigma_d(r) = \\ &= \Sigma_{b,e} \exp \left( -7.6692 \left[ \left( \frac{r}{r_{b,e}} \right)^{1/4} - 1 \right] \right) + 5.3567 \Sigma_{d,e} \exp \left( -1.6783 \frac{r}{r_{d,e}} \right) ,\end{aligned}\quad (32)$$

where quantities subscripted with  $b$  and  $d$  refer to the bulge and disk component, respectively. The total brightness predicted by this profile is

$$F_{b+d,tot} = F_{b,tot} + F_{d,tot} = 22.665 \Sigma_{b,e} r_{b,e}^2 + 11.948 \Sigma_{d,e} r_{d,e}^2 . \quad (33)$$

The relative importance of the bulge and disk component in terms of the brightness they contribute to the overall profile can be quantified by the bulge/disk ratio  $B/D$ , which, from Equations 22 and 28, can be expressed in terms of the bulge and disk parameters as

$$\frac{B}{D} = \frac{k_4 \Sigma_{b,e} r_{b,e}^2}{k_1 \Sigma_{d,e} r_{d,e}^2} = \frac{k_4}{k_1} \frac{\Sigma_{b,e}}{\Sigma_{d,e}} \frac{r_{b,e}^2}{r_{d,e}^2} = 1.8969 \rho_\Sigma \rho_r^2 , \quad (34)$$

where

$$\rho_\Sigma = \frac{\Sigma_{b,e}}{\Sigma_{d,e}} , \quad \rho_r = \frac{r_{b,e}}{r_{d,e}} . \quad (35)$$

$B/D$  is related to the more frequently used bulge/bulge+disk ratio  $B/T$  by the

$$\frac{B}{D} = \frac{B/T}{1 - B/T} . \quad (36)$$

The relation between the radii  $r_{b,e}$  and  $r_{d,e}$  and the effective radius of the bulge+disk profile  $r_{b+d,e}$ , can be determined using Equations 18 and 19, whose combination yields

$$\frac{k_4}{\Gamma(8)} \Sigma_{b,e} r_{b,e}^2 \gamma \left( 8, b_4 \left( \frac{r_{b+d,e}}{r_{b,e}} \right)^{1/4} \right) + \frac{k_1}{\Gamma(2)} \Sigma_{d,e} r_{d,e}^2 \gamma \left( 2, b_1 \frac{r_{b+d,e}}{r_{d,e}} \right) = \frac{k_4}{2} \Sigma_{b,e} r_{b,e}^2 + \frac{k_1}{2} \Sigma_{d,e} r_{d,e}^2 , \quad (37)$$

which, after trivial modifications, becomes

$$\frac{B}{D} \left[ \frac{1}{\Gamma(8)} \gamma \left( 8, b_4 \left( \frac{r_{b+d,e}}{r_{b,e}} \right)^{1/4} \right) - \frac{1}{2} \right] + \frac{k_1}{k_4} \left[ \frac{1}{\Gamma(2)} \gamma \left( 2, b_1 \rho_r \frac{r_{b+d,e}}{r_{b,e}} \right) - \frac{1}{2} \right] = 0 . \quad (38)$$

When values for the ratios  $B/D$  and  $\rho_r$  are assumed, Equation 38 can be solved numerically to obtain the corresponding values of the ratios  $r_{b,e}/r_{b+d,e}$  and  $r_{d,e}/r_{b+d,e}$ . Numerical values of the latter two ratios are given in Table 7 for some values of the former two. Now, the general bulge+disk profile can be written as

Table 7: Values of  $r_{b,e}/r_{b+d,e}$  and  $r_{d,e}/r_{b+d,e}$  for some values of  $B/D$  and  $\rho_r$ . Values calculated via Newton integration (see Section 9.7 in Press *et al.* (1992)) of Equation 38.

		$B/D$				
		0.333	0.444	0.555	0.666	0.777
$\rho_r$	0.3	0.37776903	0.39659331	0.41501285	0.43296121	0.45038387
	0.4	0.47738606	0.49489417	0.51165418	0.52767183	0.54296003
	0.5	0.57169562	0.58717625	0.60178337	0.61556793	0.62857967
	0.6	0.66216968	0.67514232	0.68725805	0.69858888	0.70920016
	0.7	0.74977666	0.75987986	0.76924321	0.77794075	0.78603748
		$B/D$				
		0.333	0.444	0.555	0.666	0.777
$\rho_r$	0.3	1.2592301	1.3219777	1.3833761	1.4432040	1.5012795
	0.4	1.1934651	1.2372354	1.2791355	1.3191796	1.3574001
	0.5	1.1433912	1.1743525	1.2035667	1.2311359	1.2571593
	0.6	1.1036161	1.1252372	1.1454301	1.1643148	1.1820002
	0.7	1.0711095	1.0855427	1.0989189	1.1113440	1.1229107

$$\Sigma_{b+d}(r) = \frac{\Sigma_{b,e}}{\Sigma_{b+d,e}} \Sigma_{b+d,e} \exp\left(-7.6692 \left[\left(\frac{r_{b+d,e}}{r_{b,e}} \frac{r}{r_{b+d,e}}\right)^{1/4} - 1\right]\right) + 5.3567 \frac{\Sigma_{d,e}}{\Sigma_{b+d,e}} \Sigma_{b+d,e} \exp\left(-1.6783 \frac{r_{b+d,e}}{r_{d,e}} \frac{r}{r_{b+d,e}}\right). \quad (39)$$

In much the same way as Equation 38, Equation 39 can be numerically solved with respect to the ratios  $\Sigma_{b,e}/\Sigma_{b+d,e}$  and  $\Sigma_{d,e}/\Sigma_{b+d,e}$  if values of the ratios  $B/D$  and  $\rho_r$  are assumed. Numerical values of the two former ratios are given in Table 8 for the same values of the latter two as in Table 7. Tables 7 and 8, combined with Equation 39, allows to write the appropriate bulge+disk profile for different values of  $B/D$  and  $\rho_r$ . The total brightness predicted by the law can then be written in terms of the bulge+disk quantities  $r_{b+d,e}$  and  $\Sigma_{b+d,e}$  as

$$F_{D,tot} = \left[ k_4 \frac{\Sigma_{b,e}}{\Sigma_{b+d,e}} \left(\frac{r_{b,e}}{r_{b+d,e}}\right)^2 + k_1 \frac{\Sigma_{d,e}}{\Sigma_{b+d,e}} \left(\frac{r_{d,e}}{r_{b+d,e}}\right)^2 \right] \Sigma_{b+d,e} r_{b+d,e}^2 \equiv k_{b+d} \Sigma_{b+d,e} r_{b+d,e}^2, \quad (40)$$

and, proceeding like for the pure bulge and disk profiles,  $\mu_{b+d,e}$  can be written as

$$\mu_{b+d,e} = 2.5 \log(k_{b+d}) + 5 \log(r_{e,[\text{as}]}) + I_{[\text{mag}]} \quad [\text{mag arcsec}^{-2}]. \quad (41)$$

Values of  $k_{b,d}$  are given in Table 9.

Table 8: Values of  $\Sigma_{b,e}/\Sigma_{b+d,e}$  and  $\Sigma_{d,e}/\Sigma_{b+d,e}$  for the same values of  $B/D$  and  $\rho_r$  as in Table 7. Values calculated from Equations 32 and 34, and from Table 7.

		$B/D$				
		0.333	0.444	0.555	0.666	0.777
$\rho_r$	0.3	1.5059000	1.6695642	1.7862309	1.8669555	1.9202392
	0.4	0.90250402	1.0169289	1.1059437	1.1750876	1.2286100
	0.5	0.61171687	0.69840479	0.76930751	0.82759966	0.87573973
	0.6	0.44733235	0.51643686	0.57490397	0.62470279	0.66737834
	0.7	0.34431760	0.40137789	0.45089086	0.49413744	0.53213802
		$B/D$				
		0.333	0.444	0.555	0.666	0.777
$\rho_r$	0.3	0.57903215	0.51357003	0.45788132	0.41020644	0.36917465
	0.4	0.61692617	0.55611501	0.50399454	0.45900376	0.41992150
	0.5	0.65336297	0.59676211	0.54778829	0.50511037	0.46768035
	0.6	0.68801330	0.63543886	0.58948209	0.54903740	0.51322600
	0.7	0.72080756	0.67220776	0.62927470	0.59111205	0.55699899

Table 9: Values of  $k_{b+d}$  for the same values of  $B/D$  and  $\rho_r$  as in Tables 7 and 8. Values calculated from Equation 40 and from Tables 6, 7 and 8.

		$B/D$				
		0.333	0.444	0.555	0.666	0.777
$\rho_r$	0.3	15.841388	16.675985	17.443019	18.140889	18.770256
	0.4	15.161182	15.816591	16.415234	16.959955	17.454163
	0.5	14.737528	15.291208	15.795789	16.255446	16.674198
	0.6	14.458169	14.948771	15.395577	15.803140	16.175547
	0.7	14.268144	14.717733	15.127242	15.501275	15.843825

## References

- Abraham, R. *et al.* (1996a). Galaxy Morphology to  $I = 25$  in the Hubble Deep Field. *Monthly Notices of the Royal Astronomical Society*, **279**, L47–52.
- Abraham, R. *et al.* (1996b). The Morphologies of Distant Galaxies. II. Classifications from the Hubble Space Telescope Medium Deep Survey. *Astronomy and Astrophysics Supplement Series*, **107**, 1–17.
- Andredakis, Y., Peletier, R., and Balcells, M. (1995). The Shape of the Luminosity Profiles of Bulges of Spiral Galaxies. *Monthly Notices of the Royal Astronomical Society*, **275**, 874.
- Binney, J. and Merrifield, M. (1998). *Galactic Astronomy*. Princeton University Press.

- Boroson, T. (1981). The Distribution of Luminosity in Spiral Galaxies. *Astrophysical Journal Supplement Series*, **46**, 177–209.
- Byun, Y. and Freeman, K. (1995). Two-Dimensional Decomposition of Bulge and Disk. *Astrophysical Journal*, **448**, 563.
- Caon, N., Capaccioli, M., M., and D’Onofrio (1993). On the Shape of the Light Profiles of Early-Type Galaxies. *Monthly Notices of the Royal Astronomical Society*, **265**, 1013–1021.
- Capaccioli, M. *et al.* (1988). Photographic and CCD Surface Photometry of nine Early-Type Galaxies. *Astronomical Journal*, **96**, 487–503.
- Capaccioli, M., Held, E., Lorenz, H., and Vietri, M. (1990). Photographic and CCD Surface Photometry of the Standard Elliptical Galaxy NGC 3379. *Astronomical Journal*, **99**, 1813–1822.
- Casertano, S. *et al.* (1995). Structural Parameters of Faint Galaxies from Prefurbishment Hubble Space Telescope Medium Deep Survey Observations. *Astrophysical Journal*, **453**, 599–610.
- de Vaucouleurs, G. (1948). Recherches sur les Nebuleuses Extragalactiques. *Annales d’Astrophysique*, **11**, 247.
- de Vaucouleurs, G. (1959). Classification and Morphology of External Galaxies. In J. Flüggé, editor, *Handbuch der Physik*, volume 53, pages 275–310. Springer Verlag.
- ESA (2000). *GAIA: Composition, Formation and Evolution of the Galaxy, Concept and Technology Study Report*. ESA–SCI(2000)4. ESA. Compiled by the GAIA Science Advisory Group.
- Freeman, K. (1970). On the Disks of Spiral and S0 galaxies. *Astrophysical Journal*, **160**, 811–830.
- Glazebrook, K., Ellis, R., Santiago, B., and Griffiths, R. (1995). The morphological identification of the rapidly evolving population of faint galaxies. *Monthly Notices of the Royal Astronomical Society*, **275**, L19–L22.
- Høg, E., Fabricius, C., Knude, J., and Makarov, V. (1999). Sky Survey and Photometry by the GAIA Satellite. *Baltic Astronomy*, **8**, 25–56. GAIA-CUO-53.
- Hubble, E. (1926). Extra-Galactic Nebulae. *Astrophysical Journal*, **54**, 321–369.
- Hubble, E. (1936). *The Realm of the Nebulae*. Yale University Press.
- Im, M., Casertano, S., Griffiths, R., and Ratnatunga, K. (1995). A Test of Galaxy Evolutionary Models through Angular Sizes. *Astrophysical Journal*, **441**, 494–504.

- Jedrzejewski, R. (1987). CCD Surface Photometry of Elliptical Galaxies — I. Observations, Reduction and Results. *Monthly Notices of the Royal Astronomical Society*, **226**, 747–768.
- Kent, S. (1985). CCD Surface Photometry of Field Galaxies. II. Bulge/Disk Decompositions. *Astrophysical Journal Supplement Series*, **59**, 115–159.
- Lattanzi, M. (1997). Stars and Galaxies at  $I = 20$ . Technical Report SAG\_MGL.03.
- Makino, J., Akiyama, K., and Sugimoto, D. (1990). On the apparent universality of the  $R^{1/4}$  law for brightness distribution in galaxies. *Publications of the Astronomical Society of Japan*, **42**, 205–215.
- Mihalas, D. and Binney, J. (1981). *Galactic Astronomy, Structure and Kinematics*. Freeman, San Francisco, second edition.
- Perryman, M. *et al.* (2001). GAIA: Composition, Formation and Evolution of the Milky Way. *Astronomy and Astrophysics*, **369**, 339–363.
- Press, W., Teukolsky, S., Vetterling, W., and Flannery, B. (1992). *Numerical Recipes in Fortran 77: The Art of Scientific Computing (Volume I of Fortran Numerical Recipes)*. Cambridge University Press.
- Prugniel, P. and Héraudeau, P. (1998). Total Magnitude, Radius, Colour Indices, Colour Gradients and Photometric Type of Galaxies. *Astronomy and Astrophysics Supplement Series*, **128**, 299–308.
- Ratnatunga, K., Griffiths, R., and Ostrander, E. (1999). Disk and Bulge Morphology of WFPC2 Galaxies: The HST Medium Deep Survey Database. *Astronomical Journal*, **118**, 86–107.
- Sandage, A. (1961). *The Hubble Atlas of Galaxies*. The Carnegie Institution of Washington, Washington D.C.
- Sersic, J. (1968). *Atlas de Galaxias Australes*. Observatorio Astronomico, Cordoba, Argentina.
- Shapley, H. and Ames, A. (1932). *A survey of the external galaxies brighter than the thirteenth magnitude*. Astronomical Observatory of Harvard College, Cambridge, Massachusetts.
- Shimasaku, K. and Fukugita, M. (1998). The History of Galaxies and Galaxy Number Counts. *Astrophysical Journal*, **501**, 578–596.
- Vaccari, M. (2000). *GAIA Galaxy Survey: Simulated Observation of Galaxies with ESA GAIA Satellite*. Master’s thesis, Department of Astronomy and Department of Physics “G. Galilei”, University of Padova. Available at <http://mimir.pd.astro.it/~mattia/research/> or upon request writing to [vaccari@pd.astro.it](mailto:vaccari@pd.astro.it).

- Vaccari, M. (2001). GAIA Galaxy Survey: a multi-colour galaxy survey with GAIA. In *Proceedings of the Summer School "GAIA: a European Space Project", held on the 13-18 May 2001 at the Ecole de Physique des Houches, Les Houches, France*, Journal de Physique IV. Editions de Physique. astro-ph/0110144.
- van den Bergh, S. (1960). A reclassification of the northern Shapley-Ames galaxies. *Publications of the David Dunlap Observatory*, **2**, 159–199.
- van den Bergh, S. (1998). *Galaxy Morphology and Classification*. Cambridge University Press.
- van den Bergh, S. *et al.* (1996). A Morphological Catalog of Galaxies in the Hubble Deep Field. *Astronomical Journal*, **112**, 359–368.
- Williams, R. *et al.* (1996). The Hubble Deep Field: Observations, Data Reduction and Galaxy Photometry. *Astronomical Journal*, **112**, 1335–1389.